Journal of Hazardous Materials 181 (2010) 112–120

Contents lists available at ScienceDirect

Journal of Hazardous Materials

journal homepage: www.elsevier.com/locate/jhazmat

The decolorization of Acid Orange II in non-homogeneous Fenton reaction catalyzed by natural vanadium–titanium magnetite

Xiaoliang Liang[a,b], Yuanhong Zhong[a,b], Sanyuan Zhu[a], Jianxi Zhu[a], Peng Yuan[a], Hongping He[a,*], Jing Zhang[c]

[a] Guangzhou Institute of Geochemistry, Chinese Academy of Sciences, 510640, China
[b] Graduate University of the Chinese Academy of Sciences, Beijing 100049, China
[c] Institute of High Energy Physics, Chinese Academy of Sciences, Beijing 100049, China

ARTICLE INFO

Article history:
Received 9 February 2010
Received in revised form 22 April 2010
Accepted 24 April 2010

Keywords:
Natural vanadium–titanium magnetite
Non-homogeneous Fenton reaction
Degradation
Acid Orange II
Catalyst

ABSTRACT

The catalytic activity of natural vanadium–titanium magnetite was investigated in the decolorization of Acid Orange II by non-homogeneous Fenton process. The natural catalysts purified by magnetic separation were characterized using X-ray diffraction (XRD), polarizing microscope, X-ray absorption fine structure (XAFS) analysis and Mössbauer spectroscopy. The obtained results show that the natural samples after magnetic separation mainly contain titanomagnetite, with a small amount of ilmenite and chlorite. Titanomagnetite is doped with vanadium, whose the valency is mainly +3 and occupies the octahedral site. Batch decolorization studies were performed to evaluate the influences of various experimental parameters like initial pH, the amount of catalyst and initial concentration of hydrogen peroxide on the decolorization efficiency of Acid Orange II. The decolorization of the dye mainly relied on degradation. The degradation efficiency was strongly dependent on pH of the medium where it increased as the pH decreased in acid range. The increase of catalyst and hydrogen peroxide could accelerate the degradation. The catalytic property of natural vanadium–titanium magnetite in the degradation of Acid Orange II was stronger than that of synthetic magnetite (Fe_3O_4). The catalytic activity of the natural samples was greatly related to the titanomagnetite content. The degradation process was dominated by heterogeneous Fenton reaction, complying with pseudo-first-order rate law. The natural catalyst has a good catalytic stability.

1. Introduction

Recently, non-homogeneous Fenton technologies using iron oxides as catalysts have received a great deal of attention [1–5]. A variety of organic pollutants (e.g. phenol, dye and pesticide) could be effectively degraded through non-homogeneous process using iron oxides as catalysts, including goethite, lepidocrocite, hematite and magnetite [6–13]. Compared with other iron oxides, the catalytic activity of magnetite in these non-homogeneous Fenton systems seems more interesting since magnetite contains both Fe^{2+} and Fe^{3+}, the crucial cations for initiation of Fenton reaction according to the classical Haber–Weiss mechanism [14–16]. Also, magnetite is magnetic and can be easily separated from the terminal solution by magnetic separation, making it available for flow-bed technologies.

With the advantages of strong catalytic activity, wide distribution, great reserves and excellent environmental harmony, magnetite is recognized as an ideal catalytic material [17]. In the structure of magnetite, iron can be replaced by some transition metals (e.g. Ti, V, Cr, Mn, Co and Ni) while maintaining the inverse spinel structure [18–21]. The isomorphous substitution plays a great influence on the activity of the resulting magnetite. The introduction of transition metals such as Ti, Cr, Mn and Co in the spinel lattice can strongly improve the catalytic properties of magnetites and also influence their thermal stabilities. For example, the doping of Cr can directly enhance the catalytic property in the H_2O_2 decomposition and methylene blue degradation while it also leads to a promotion in the heat stability [19].

So far most relative studies have just focused on the catalytic activity of non-doped magnetite (Fe_3O_4) and transition metal doped magnetites ($Fe_{3-x}M_xO_4$, M = Cr, Co, Mn, Ni), which are all single-phase materials synthesized in the laboratory [14,19,22,23]. However, little attention has been paid to the catalytic property of natural magnetite. In fact, magnetite naturally doped with various transition metals widely exists on the earth surface, which may be an immense resource of catalyst and greatly influence the geochemical processes of organic pollutants.

* Corresponding author. Tel.: +86 20 85290257, fax: +86 20 85290708.
E-mail address: hehp@gig.ac.cn (H. He).

0304-3894/$ – see front matter © 2010 Elsevier B.V. All rights reserved.
doi:10.1016/j.jhazmat.2010.04.101

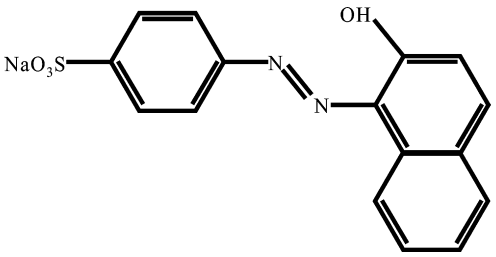

Fig. 1. The chemical structure of Acid Orange II.

In this study, the catalytic activity of natural vanadium–titanium magnetite and the relative controlling factors were investigated in the decolorization of Acid Orange II. The main oxidation mechanism in this system was non-homogeneous reaction with hydrogen peroxide as oxidant, usually present and easily decomposed in rainwater [24]. Therefore, this study primarily concentrated on the degradation of dye catalyzed by natural magnetite using hydrogen peroxide as oxidant and it also played a simulation of the decomposition of pollutants by natural mineral. The new insights obtained in this study are of high importance for the development of novel materials in environmental decontamination and good understanding of the transfer and transformation of pollutants on the earth surface.

2. Experimental

2.1. Materials

All chemicals and reagents used in this study are of analytical grade. Acid Orange II ($C_{16}H_{11}N_2SO_4Na$, C.I. 15510, C.I. Acid Orange 7, M.W.: 350.32, certified pure) was purchased from Shanghai Chemical Reagent Company and used as received. Its chemical structure is shown in Fig. 1. Deionized water was used to make the dye solutions of desired concentration.

The samples of natural vanadium–titanium magnetite (named as M1, M2 and M3) were collected from Pan-Xi region, a famous iron deposit in Sichuan Province, China. These samples were purified by magnetic separation before characterization and decolorization experiment. After magnetic separation, quartz and most of the clay minerals were eliminated. Magnetite (Fe_3O_4, named as M0) was synthesized by means of a precipitation–oxidation method with sulfate as starting material, which was pro rata oxidized to ferric salts by $NaNO_3$ after alkalinizing with NaOH. The synthesis procedure of M0 has been reported in detail in other Refs. [25,26]. All the samples were ground and passed through a 200 mesh screen (0.074 mm).

2.2. Characterization of magnetites

Powder X-ray diffraction patterns (PXRD) were recorded between 10° and 80° (2θ) at a step of 1° min^{-1} using a Bruker D8 advance diffractometer with Cu Kα radiation (40 kV and 40 mA). The mineral composition in the natural magnetite was obtained from XRD patterns by *K* value method.

Natural magnetite M2 was observed under polarizing microscope Leica DMRX, using orthogonal polarization under transmitted light, with 10 × 63 as power of magnification.

The V K-edge X-ray absorption fine structure (XAFS) spectra of natural vanadium–titanium magnetite M3 and reference compounds were collected on beamline 1W1B of Beijing Synchrotron Radiation Facility (BSRF). The BSRF storage ring is operated at the electron energy of 2.2 GeV with beam current of 250 mA. The 1W1B is a focused X-ray beamline, using a Si (1 1 1) double crystal monochromator. The V K-edge XAFS spectra of V_2O_3, VO_2 and V_2O_5 reference compounds were measured in transmission mode, and that of M3 was collected in fluorescence mode with a Lytle detector and a Ti foil filter.

For ^{57}Fe Mössbauer measurement, 250–335 mg of the powder sample without any chemical pretreatment was gently pressed into a brass sample holder (16 mm in diameter, 1 mm thick). The sample holder was closed on two ends with iron free plastic tap. The Mössbauer spectra were obtained with a Mössbauer spectrometer Austin Science S-600 using a γ-ray source of 1.11 GBq ^{57}Co/Rh at a consistent temperature (293 K). Spectra were fitted to Lorentzian lineshapes using standard line shape fitting routines with a personal computer. Half-width (HW) and peak intensity of each quadruple doublet was constrained to be equal. Isomer shifts (IS) were expressed with respect to the centered of the spectrum of metallic iron foil.

2.3. Decolorization of azo-dye Acid Orange II

The experiments were carried out in a conical flask (containing 200 mL of reaction solution). The temperature was controlled to 25 °C. The dosage of catalyst was 0–2.0 g L^{-1} while the concentrations of Acid Orange II and H_2O_2 were 0.2 mmol L^{-1} and 0–20 mmol L^{-1}, respectively. All the experiments were carried out under constant stirring to make the catalyst well dispersed. The pH of solution was adjusted by H_2SO_4 and NaOH. Before degradation reaction, the suspension containing catalyst and Acid Orange II was stirred for 1 h to achieve adsorption equilibrium. Then the degradation reaction was initiated by adding H_2O_2 into Acid Orange II solution.

At given intervals of degradation, each sample was analyzed by UV–vis spectroscopy UV-7504 at a wavelength of 484 nm, the maximum absorption wavelength of Acid Orange II. The concentration of Acid Orange II was converted through the standard curve method of the dye. The UV–visible absorption spectra were measured by PerkinElmer Lamboda 850 for each sample. Total organic carbon (TOC) concentration was analyzed in a Shimadzu TOC-VCPH analyzer to evaluate the mineralization of dyes. Before centrifugation and analysis, all the samples were immediately treated with equal volume of prepared scavenging reagent in order to stop the reaction in the samples. The prepared scavenging reagent contained 0.1 mol L^{-1} Na_2SO_3, 0.1 mol L^{-1} KH_2PO_4, 0.1 mol L^{-1} KI and 0.05 mol L^{-1} NaOH, to obtain accurate TOC values [27,28].

Four hours after the degradation experiment started, the reaction solution was filtered through a Millipore filter (pore size 0.22 μm) to remove the solid catalysts. Then H_2O_2 and Acid Orange II were added to the filtrate, to build a homogeneous Fenton reaction system catalyzed by dissolved iron [29]. The concentrations of Acid Orange II and H_2O_2 were 0.2 mmol L^{-1} and 10 mmol L^{-1}, respectively. The operation of homogeneous Fenton reaction was similar to that of heterogeneous Fenton reaction mentioned above.

Four hours after the degradation experiment started, the near-infrared diffuse reflectance spectroscopy of final degradation products was recorded on a Bruker Vector 70 Fourier transform infrared spectrometer. The infrared signal was obtained by a MCT detector. Diffuse reflectance spectra were recorded at 4 cm^{-1} resolution with 64 scans over the spectral range 1750–1000 cm^{-1}, the main wavelength range of the absorption peaks of Acid Orange II.

3. Results and discussion

3.1. Characterization of catalysts

3.1.1. XRD, XAFS and polarizing microscope

XRD patterns of synthesis magnetite (M0) and natural vanadium–titanium magnetites (M1, M2 and M3) are shown in

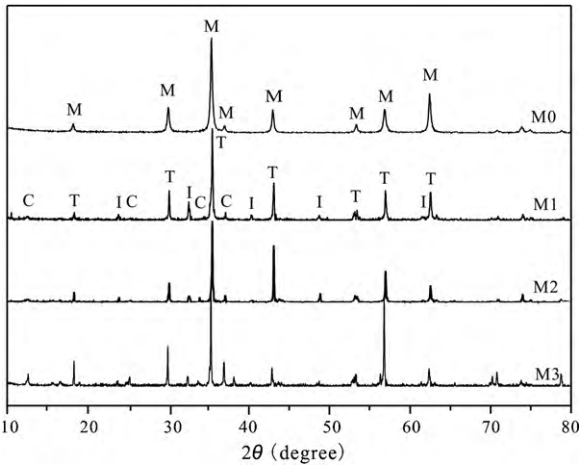

Fig. 2. X-ray diffraction patterns of series of magnetites (M, magnetite; T, titanomagnetite; I, ilmenite; C, chlorite).

Fig. 2. The characteristic reflections of M0 well correspond to the standard card of magnetite (JCPDS: 19-0629, not shown). This indicates that synthetic magnetite has spinel structure [30,31]. The XRD patterns of the natural samples show that all the natural vanadium–titanium magnetites consist of titanomagnetite ($2\theta = 35.5^\circ$, 43.1°, 62.6°), ilmenite ($2\theta = 32.6^\circ$, 40.1°, 23.8°) and chlorite ($2\theta = 12.5^\circ$, 25.4°, 34.0°). Ilmenite and chlorite are the common minerals coexisting with titanomagnetite in natural vanadium–titanium magnetites.

The image of M2 under polarizing microscope is provided in Fig. 3. The black grains are titanomagnetite and ilmenite, coexisting as intergrowth. The transparent ones are chlorite, with the granule diameter ranging from 2 μm to 7 μm, extensively dispersed in the samples.

From previous studies, the titanomagnetite in Pan-Xi region is vanadium-rich titanomagnetite [21,32]. The normalized XANES spectra for vanadium K-edge of M3 and reference compounds are shown in Fig. 4. The V K-edge XANES of these oxides exhibit a pre-edge absorption feather from V_2O_3 to V_2O_5, followed by a strong peak in the vicinity of about 20 eV. The vanadium K-edge of M3 displays a rather different feather from those vanadium oxides. A weak pre-edge absorption appears, and two other should be observed in the absorption edge. This indicates vanadium in titanomagnetite is impossible to exist as these vanadium oxides. Because the shape of absorption edge is affected by the symmetry of vanadium and the energy position of the absorption edge is difficult to define, the valence state of vanadium in M3 cannot be determined by chemical shifts. The correlations between normalized pre-edge peak area and its centroid position have been studied by Chaurand et al. [33], and

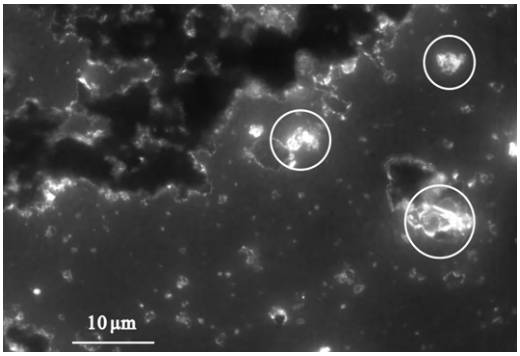

Fig. 3. Image of M2 under polarizing microscope (○, chlorite).

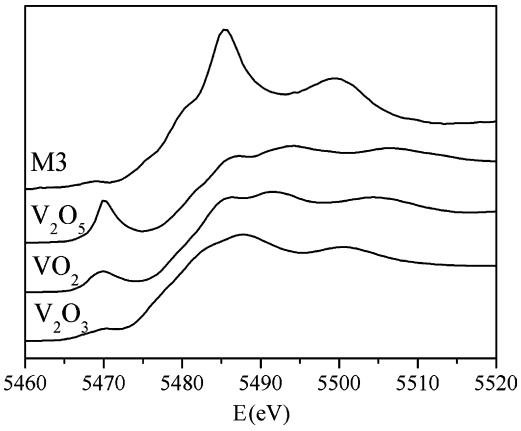

Fig. 4. XANES of vanadium oxides and natural vanadium-titanium magnetite M3.

can be used to determine to the valence state and symmetry. For vanadium in the natural magnetite, the pre-edge peak area is rather low, and the centroid is located at 5468.8 eV, about 3.8 eV above the absorption edge of vanadium metal (5465.0 eV). This result suggests vanadium in natural sample is trivalent and occupies the octahedral site of magnetite.

The lattice parameter a_0 of M0 is 0.8394 nm while that of titanomagnetite phase in M1, M2 and M3 are 0.8387 nm, 0.8384 nm and 0.8397 nm, respectively. The lattice parameter a_0 of titanomagnetite is quite close to that of synthetic Fe_3O_4, ascribed to the close value of cationic radii for Ti^{4+} (60 pm), V^{3+} (64 pm) and displaced Fe^{3+} (65 pm) in the octahedral site [26,30,34].

Calculated using the Scherrer equation, the crystallite sizes of M0, M1, M2 and M3 are 34 nm, 122 nm, 65 nm and 106 nm, respectively. This shows that the crystal sizes of natural samples are larger than that of synthetic magnetite. Calculated by *K* value method, the contents of magnetite, titanomagnetite, ilmenite and chlorite in four samples are listed in Table 1. It can be seen that the titanomagnetite content in these three natural samples increases from M1 to M2 and then to M3.

3.1.2. Mössbauer spectroscopy

The Mössbauer spectra (Fig. 5) and Mössbauer spectral parameters of M0 (Table 2) indicate the formation of magnetite with hyperfine field (B_{hf}) of 48.70 T (tetrahedral site A) and 45.36 T (octahedral site B) and isomer shifts (IS) 0.331 mm s^{-1} and 0.603 mm s^{-1}, respectively [35,36]. Also, a signal with B_{hf} 50.22 T, IS 0.357 mm s^{-1} and the relative area of 10.2% suggests partial oxidation of magnetite to maghemite γ-Fe_2O_3 [37].

For natural vanadium–titanium magnetite, the Mössbauer spectra (Fig. 5) and parameters (Table 2) also show the typical spectra of the cubic spinel structure, related to existence of titanomagnetite. Also, a signal with IS 1.07–1.10 mm s^{-1} and the relative area of 12.4–16.9% is ascribed to the presence of ilmenite. However, the chlorite does not have Mössbauer signal, due to its low iron concentration.

Table 1
Content of minerals in series of magnetites.

	M^a (%)	T^b (%)	I^c (%)	C^d (%)
M0	100	0	0	0
M1	0	66	20	14
M2	0	72	5	23
M3	0	76	12	12

[a] Magnetite.
[b] Titanomagnetite.
[c] Ilmenite.
[d] Chlorite.

Table 2
Mössbauer parameters for the series of magnetite.

Sample	Phase	IS (mm/s) (±0.002)	QS (mm/s) (±0.004)	B_{hf} (T) (±0.004)	Relative area (%)
Fe_3O_4	Fe_3O_4 (A)	0.331	−0.004	48.70	45.9
	Fe_3O_4 (B)	0.603	0.060	45.36	43.9
	γ-Fe_2O_3	0.357	0.034	50.22	10.2
M1	Fe_3O_4 (A)	0.274	0.003	48.89	26.1
	Fe_3O_4 (B)	0.660	−0.030	45.74	57.0
	$FeTiO_3$	1.072	0.753	–	16.9
M2	Fe_3O_4 (A)	0.234	−0.089	49.04	32.0
	Fe_3O_4 (B)	0.708	0.057	46.62	55.6
	$FeTiO_3$	1.104	0.756	–	12.4
M3	Fe_3O_4 (A)	0.295	0.006	49.00	30.7
	Fe_3O_4 (B)	0.660	−0.017	45.75	56.4
	$FeTiO_3$	1.072	0.696	–	12.9

3.2. Catalytic activity

3.2.1. Effect of initial pH

In this study, the decolorization of Acid Orange II was attributed to two aspects: on one hand, magnetites could act as catalyst in the non-homogeneous Fenton reaction, generating •OH radicals that attacked the dye. On the other hand, the adsorption of the dye on the catalyst surface led to a limiting color removal in this study.

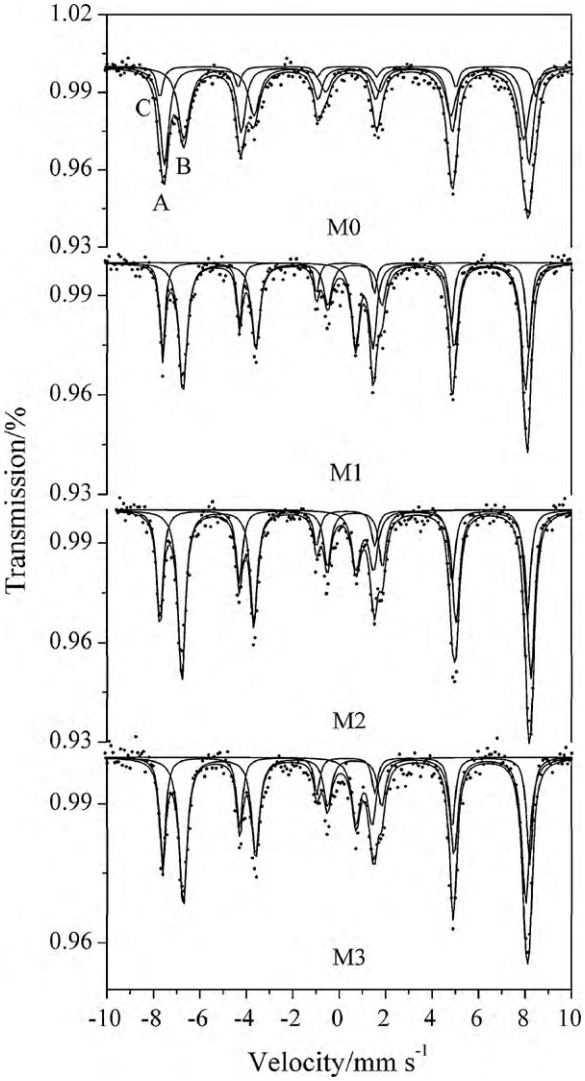

Fig. 5. Mössbauer spectra of series of magnetites.

The effect of initial solution pH on the decolorization rate of Acid Orange II is shown in Fig. 6. It can be seen that under different pH, the adsorbed amount of the dye was quite low. Therefore, the decolorization of the dye was mainly dependent on degradation. When the initial pH was 3.0, Acid Orange II could be quickly degraded in 180 min under the adopted conditions. But as the initial pH rose, the degradation became much slower. After 360 min, the decolorization rates of Acid Orange II with the initial pH at 4.0 and 5.0 were 30% and 8%, respectively. The obtained results indicated that the increase of initial pH led to a much lower degradation rate.

It has been confirmed that low pH promotes the stability of hydrogen peroxide and slowed its decomposition [38]. Therefore, the decrease of pH would slow the decomposition of H_2O_2, which may slow the decolorization process. However, in this study the decrease of initial pH has led to a much larger degradation rate. The previous studies have approved that the degradation rate of pollutants correlates to the adsorption behavior of pollutants on the catalysts [29]. A larger adsorbed amount favors the degradation of pollutants. In this study, the solution pH greatly influenced the adsorption through affecting the surface complexation reactions and the electrostatic interactions between the dye and magnetite [39]. Since the point of zero charge (pH_{pzc}) of natural magnetite was 6.8–8.0, the magnetite exhibited a positive zeta potential at pH values lower than pH_{pzc}, due to the formation of positive Fe–OH_2^+ surface groups that increased as pH decreased [40]. On the other hand, a pK_{a1} value of 1.0 for the –SO_3H group and a pK_{a2} value of 11.4 for the naphthalene of Acid Orange II, it could be conducted that in the pH range studied most of the dye was negative charged

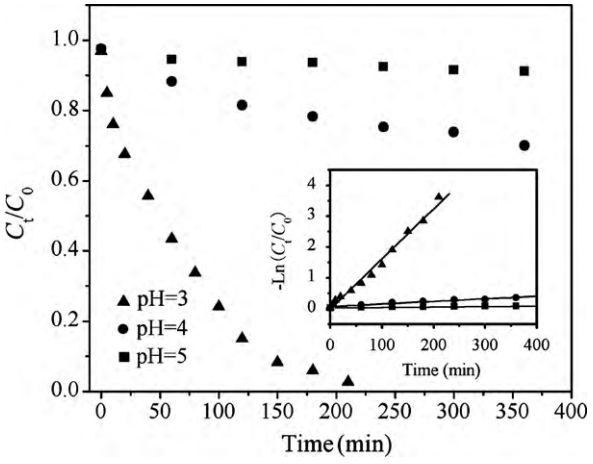

Fig. 6. The effect of initial pH value on the decolorization efficiency of Acid Orange II. Inset: fitted by pseudo-first-order rate law (C_0 = 0.2 mmol L^{-1}, 10 mmol L^{-1} of H_2O_2, 1.0 g L^{-1} of M2, 200 mL, 25 °C).

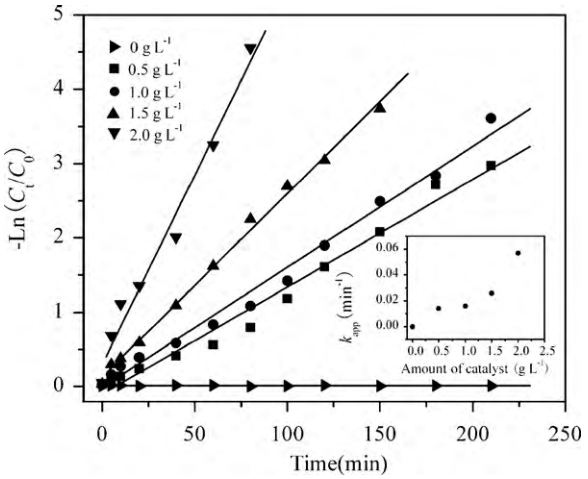

Fig. 7. The effect of amount of catalyst on the decolorization efficiency of Acid Orange II. Inset: correlation of the apparent pseudo-first-order rate constant with amount of catalyst (C_0 = 0.2 mmol L^{-1}, 10 mmol L^{-1} of H_2O_2, 200 mL, pH = 3.0, 25 °C, catalyst: M2).

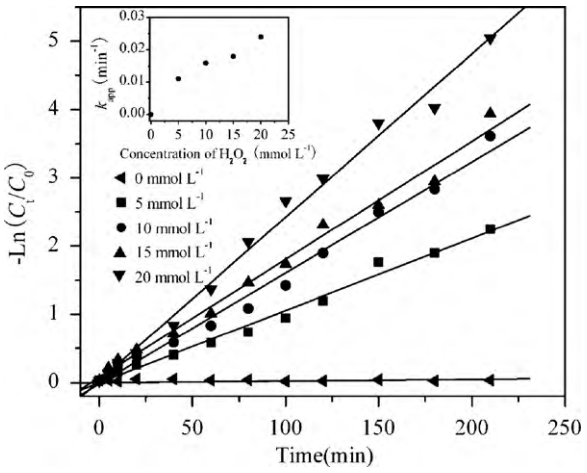

Fig. 8. The effect of H_2O_2 concentration on the decolorization efficiency of Acid Orange II. Inset: correlation of the apparent pseudo-first-order rate constant with H_2O_2 concentration (C_0 = 0.2 mmol L^{-1}, 1.0 g L^{-1} of M2, 200 mL, pH = 3.0, 25 °C).

[41]. Therefore, lower pH could increase the electrostatic attraction between dye molecules and surfaces of adsorbents and favor the adsorption reaction. With the decrease of pH, the increase of adsorbed amount led to higher degradation rate. It is necessary to mention that with decrease of pH in the solution, the amount of Fe leaching would increase, which speeds the production of •OH through homogenous Fenton reaction. The contribution of homogenous Fenton reaction to the whole decolorization process would be discussed below. Moreover, in Fig. 6 all the decolorization processes complied with pseudo-first-order rate law.

3.2.2. Effect of catalyst dosage

As expected, Acid Orange II degradation rate increased as the amount of employed catalyst increased (Fig. 7), due to the increasing active sites for H_2O_2 decomposition and dye adsorption. Similarly, in Fig. 7 all the degradation processes catalyzed by the changed amount of magnetite complied with pseudo-first-order rate law. However, the relationship between apparent pseudo-first-order rate constant (k_{app}) and catalyst amount did not show a linear relationship, which may be ascribed to the competition between the dye and H_2O_2 for the active sites on catalyst surface.

3.2.3. Effect of the hydrogen peroxide concentration

The effect of hydrogen peroxide was analyzed by varying its initial concentration between 0 mmol L^{-1} and 20 mmol L^{-1} (Fig. 8). According to the previous study, 42 mol of H_2O_2 are theoretically needed for complete degradation of 1 mol of the dye [42]:

$$C_{16}H_{11}N_2SO_4Na + 42H_2O_2 \rightarrow 16CO_2 + 46H_2O + 2HNO_3 + NaHSO_4 \quad (1)$$

Based on this equation, the necessary amount of H_2O_2 in the present study for complete degradation of 0.2 mmol L^{-1} of Acid Orange II is 8.4 mmol L^{-1}. When the concentration of H_2O_2 was 5 mmol L^{-1}, the degradation process was very slow due to lack of adequate oxidant. As the concentration of H_2O_2 increased to 10 mmol L^{-1}, the process was significantly accelerated, for more radicals were formed. When the H_2O_2 concentration increased to 15 mM, the rate constant did not increase greatly, due to the well-known hydroxyl radicals scavenging effect [42]:

$$H_2O_2 + {}^{\bullet}OH \rightarrow H_2O + {}^{\bullet}O_2H \quad (2)$$

Such reaction reduced the amount of hydroxyl radicals and caused the degradation rate to drop. Although another radical ($^{\bullet}O_2H$) was produced, its oxidation potential was much smaller than that of the •OH species. Therefore, it made the reaction slow-down through the rate constant still increased. However, when the H_2O_2 concentration increased to 20 mM, the rate constant turned to obviously increase. From previous study [43], the increase of H_2O_2 dosage would increase the dissolved iron concentration under acid condition and induce the homogeneous catalytic oxidation. It may be the main reason for this phenomenon.

Otherwise, experiments were carried out in presence of magnetite or H_2O_2 alone (Figs. 7 and 8). The result showed that H_2O_2 or magnetite alone was not sufficient for the degradation of this dye.

3.2.4. Degradation of Acid Orange II by series of magnetite

The decolorization processes of Acid Orange II using four samples as catalysts are shown in Fig. 9. Before the addition of H_2O_2, the decolorization of Acid Orange II only relied on adsorption. It can be seen that the decolorization rate just by adsorption was quite low, below 5%. After the addition of H_2O_2, Acid Orange II could be degraded through non-homogeneous Fenton reaction. 180 min later, the decolorization rates of Acid Orange II by M0, M1, M2 and M3 were 72%, 89%, 94% and 98%, respectively. Since the decolorization rate of Acid Orange II just by adsorption was quite low, the decolorization of the dye mostly depended on the degradation process.

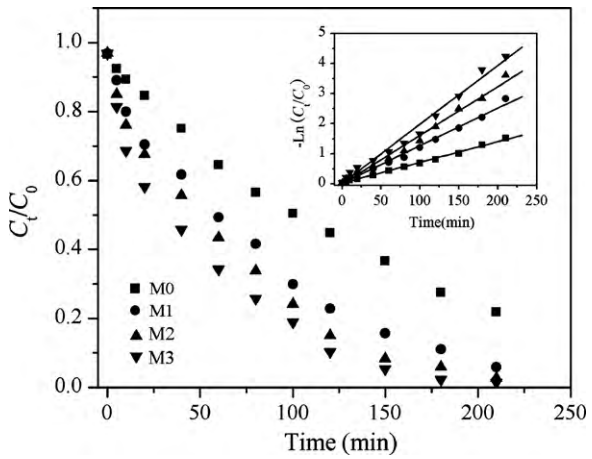

Fig. 9. Kinetic curves for Acid Orange II decolorization catalyzed by series of magnetites in the presence of H_2O_2. Inset: fitted by pseudo-first-order rate law (C_0 = 0.2 mmol L^{-1}, 10 mmol L^{-1} of H_2O_2, 1.0 g L^{-1} of catalyst, 200 mL, pH = 3.0, 25 °C).

The degradation of Acid Orange II using magnetite as catalyst corresponded to the •OH mechanism [44–46]. H_2O_2 was activated by the cations on magnetite surface via a Haber–Weiss mechanism to form radical •OH:

$$H_2O_2 + S \rightarrow {}^{\bullet}OH + OH^- + S^+ \quad (3)$$

In this equation, S and S^+ denote adsorption location and oxidized location, respectively. It has been certified that Eq. (3) follows pseudo-first-order kinetic rate law [47].

The degradation of the dye by •OH was typically described as a second-order reaction:

$$\frac{dC_t}{dt} = -kC[{}^{\bullet}OH] \quad (4)$$

where C and [•OH] are concentrations of Acid Orange II and hydroxyl radical, respectively. k is the second-order rate constant, and t is the reaction time. By assuming that •OH instantaneous concentration was constant, the kinetics of dye degradation could be described according to the pseudo-first-order equation as given below [28]:

$$\frac{dC_t}{dt} = -k_{app}C_t \quad (5)$$

$$k_{app} = k[{}^{\bullet}OH] \quad (6)$$

$$-\ln(C_t/C_0) = k_{app}t \quad (7)$$

where C_0 is the initial concentration of Acid Orange II and k_{app} is the apparent pseudo-first-order rate constant (min^{-1}). The k_{app} constants were obtained from the slopes of the straight lines by plotting $-\ln(C_t/C_0)$ as a function of time t, through regression [48]. Good correlation coefficients ($r^2 > 0.98$) were obtained in our systems (Figs. 6–9).

The apparent pseudo-first-order rate constant k_{app} for M0, M1, M2 and M3 are 0.0071 min^{-1}, 0.012 min^{-1}, 0.016 min^{-1} and 0.019 min^{-1}, respectively. It can be seen that the catalytic activity of natural vanadium–titanium magnetite is stronger than that of synthetic magnetite Fe_3O_4. It is quite interesting that catalytic activity of pure magnetite is inferior to that of natural magnetite, although the content of titanomagnetite in natural samples is just 66–76%. The higher catalytic activity of natural magnetite is related to the presence of titanium and vanadium in the magnetite. Previous researches have revealed that transition metal cations (e.g. Mn^{2+}, Cr^{3+} and Co^{2+}) replacing the ferrous and ferric ions in magnetite can improve the catalytic activity of magnetite in heterogeneous Fenton reactions, by activating H_2O_2 to produce •OH and accelerating the electron transfer during the reaction [14,19,49,50]. It also explains the effect of titanium and vanadium on the catalytic activity of natural titanium–vanadium magnetite.

The correlation of k_{app} with the content of three minerals in natural samples is shown in Fig. 10. The constant k_{app} increases remarkably with the increase of titanomagnetite content in the natural samples. The correlation of k_{app} with titanomagnetite content approximately matches a nice linear fit ($r^2 = 0.999$). On the contrary, the correlations of k_{app} with the content of other minerals in natural samples do not show good relationship. Moreover, since titanomagnetite is the main mineral in natural vanadium–titanium magnetite, this implies that titanomagnetite would be the most active ingredient in catalytic experiment.

When the solution pH value is above 4.0, the amount of dissolved iron is so low that the effect of homogeneous Fenton reaction on the degradation process can be neglected [51]. In this study, the initial solution pH was 3.0. Therefore, under this condition, the contribution of homogeneous Fenton reaction catalyzed by dissolved iron to the whole degradation process may be quite important to the reaction mechanism. Hence, a special experiment was conducted as described in the Section 2, to investigate the contribution from

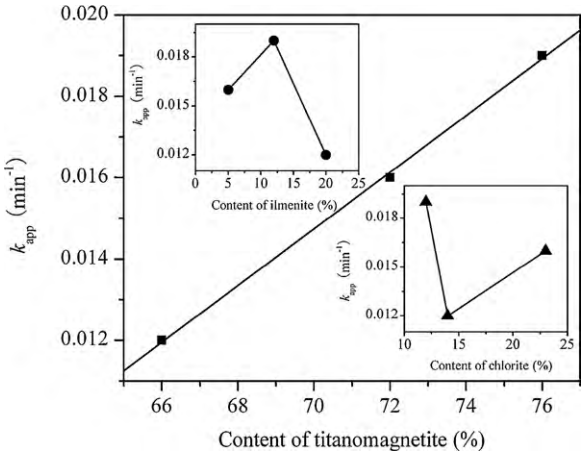

Fig. 10. Correlation of the apparent pseudo-first-order rate constant with content of three minerals in natural samples.

the homogeneous Fenton reaction. When the non-homogeneous Fenton reaction finished, the pH of the solution was 2.88–2.96, related to the presence of some degradation products. The homogeneous Fenton reaction catalyzed by the dissolved iron is shown in Fig. 11. The decolorization rate of Acid Orange II through homogeneous Fenton reaction was below 10% after 180 min. Thus, it could be observed that the effect of homogeneous Fenton reaction on the degradation process can be neglected. The whole decomposition of Acid Orange II by natural magnetite was dominated by heterogeneous Fenton reaction.

3.2.5. The mineralization process of Acid Orange II

To investigate the mineralization during the degradation of Acid Orange II by natural samples in the presence of H_2O_2, the mineralization process in the reaction system catalyzed by M3 were recorded as shown in Fig. 12. Mineralization rate is the percentage of organic compound transformed to inorganic compound, calculated as below:

$$\text{Mineralization rate} = (T_0 - T_t) \times \frac{100\%}{T_0}$$

where T_0 and T_t are the initial TOC concentration and instantaneous TOC concentration, respectively.

From Fig. 12, the mineralization of Acid Orange II was much slower than its decolorization. Four hours after the reaction started,

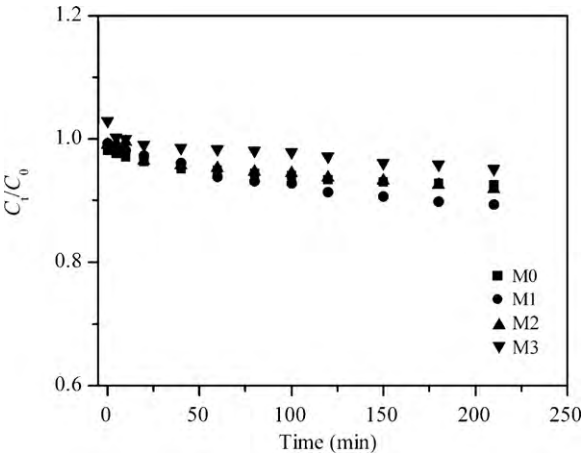

Fig. 11. Kinetic curves for Acid Orange II decolorization catalyzed by the dissolved iron ion in the presence of H_2O_2 ($C_0 = 0.2$ mmol L^{-1}, 10 mmol L^{-1} of H_2O_2, 200 mL, 25 °C).

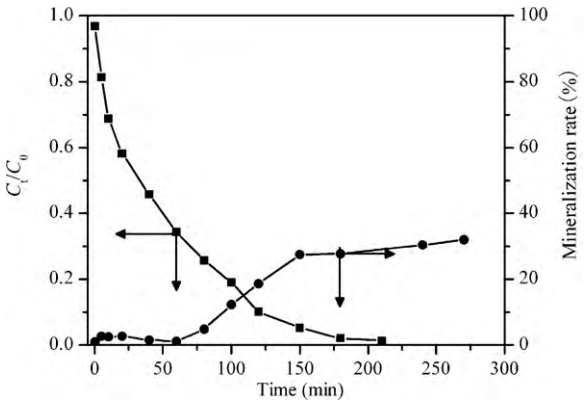

Fig. 12. Decolorization and mineralization of Acid Orange II catalyzed by M3 in the presence of H_2O_2 (C_0 = 0.2 mmol L^{-1}, 10 mmol L^{-1} of H_2O_2, 1.0 g L^{-1} of M3, 200 mL, pH = 3.0, 25 °C).

the mineralization rate of Acid Orange II was about 30%. But at the same time the decolorization of Acid Orange II was nearly 100%. So it could be inferred that some achromatic medium products was made during the degradation process.

In order to investigate the degradation products, the temporal evolution of UV–vis spectra recorded during the decolorization of Acid Orange II by M3 in the presence of H_2O_2 is shown in Fig. 13. The decrease in intensity of the peaks at 200 nm is related to the decomposition of H_2O_2. And Acid Orange II has five absorption peaks in which two peaks in visible region and three in ultraviolet region. In visible region, a major peak locates at 484 nm and a shoulder peak locates at 430 nm due to the hydrazone form and azo form of Acid Orange II, respectively. The other three peaks in ultraviolet region are assigned to the aromatic ring, among which the peaks at 228 nm and 310 nm in ultraviolet region are ascribed to the benzene and naphthalene rings of the dye, respectively. The results show that the intensity of the 484 nm and the 430 nm absorption peaks decreased rapidly with the reaction proceeding, indicating that the •OH radical firstly attacked azo groups and destructed the N=N bond [52,53]. And the intensity of the 310 nm and 228 nm absorption peaks, related to the naphthyl and benzene, respectively [54], gradually decreased, which could be inferred that these two ring were gradually broken. It confirms the fact that N=N bond is easier to be destructed than aromatic rang structure and also explains why mineralization of Acid Orange II was much slower than its decolorization. Moreover, no new absorption peaks appeared.

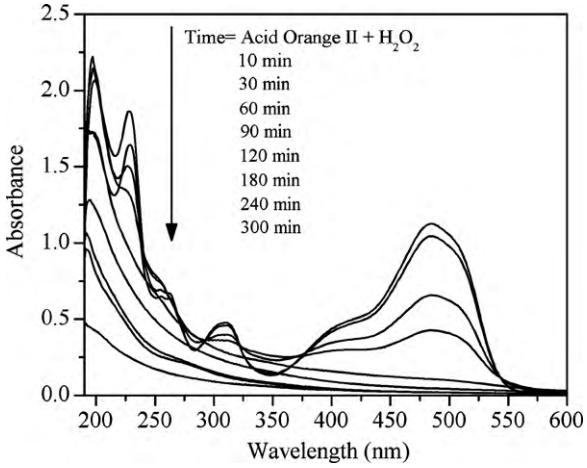

Fig. 13. UV–vis spectral changes of Acid Orange II in decolorization process as a function of reaction time (C_0 = 0.2 mmol L^{-1}, 10 mmol L^{-1} of H_2O_2, 1.0 g L^{-1} of M3, 200 mL, pH = 3.0, 25 °C).

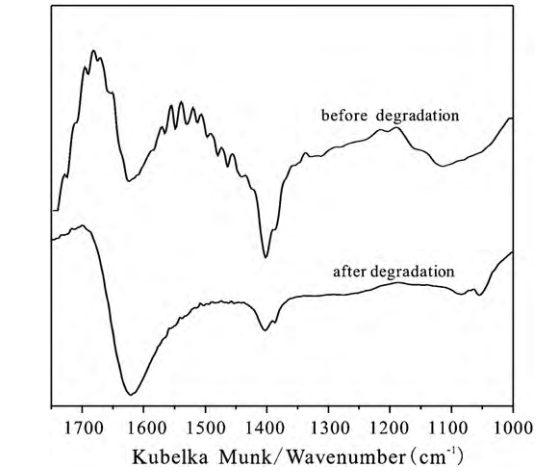

Fig. 14. Near-infrared diffuse reflectance spectroscopy of Acid Orange II and its degradation products in the solution.

The content of degradation product has also been analyzed by near-infrared diffuse reflectance spectroscopy (Fig. 14). The bands located at 1600–1450 cm^{-1} (aromatic C=C stretching), 1623 cm^{-1} (C=N stretching), 1508 cm^{-1}(N–H bending), 1452 cm^{-1} (N–N stretching), 1000–1250 cm^{-1} (S–O stretching and aromatic =C–H bending), respectively represent the characteristic absorption peaks of Acid Orange II in the infrared region [39]. After degradation, most of these bands greatly lessened in intensity or disappeared, indicating that drastic destruction happened. However, some bands did not disappeared, related to the uncompleted destruction of some aromatic group and inadequate mineralization, which well corresponds to the TOC result.

3.2.6. *The stability of natural magnetite catalyst*

Stability is an important property for effective catalyst. The stability of M3 (the most active catalyst in this study) was investigated by recycle experiment. After each recycling, the catalyst was treated by centrifugation, dried and reused. From Fig. 15, it can be found that the catalytic activity of M3 was still strong after three cycles. The decolorization rates of the dye were 98%, 93% and 90% after 180 min for cycle 1, 2 and 3, respectively. All three cycles complied with the pseudo-first-order rate law. It indicates that the natural vanadium–titanium magnetite has a good long-term sta-

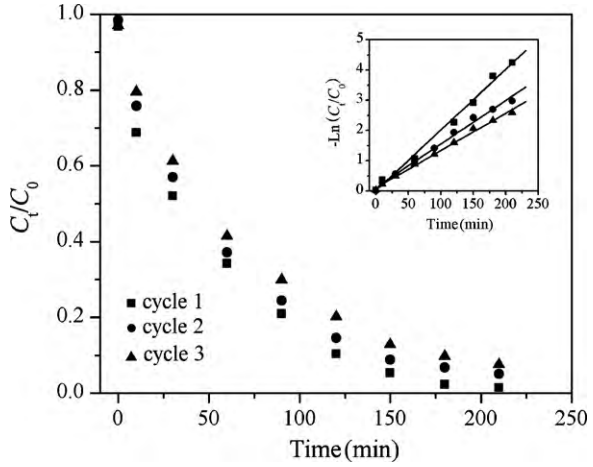

Fig. 15. Decolorization of Acid Orange II in the recycle experiment. Inset: fitted by pseudo-first-order rate law (C_0 = 0.2 mmol L^{-1}, 10 mmol L^{-1} of H_2O_2, 1.0 g L^{-1} of M3, 200 mL, pH = 3.0, 25 °C).

bility and activity. The small decrease of catalytic activity was due to dissolution of iron in natural magnetite.

4. Conclusion

The natural vanadium–titanium magnetite purified by magnetic separation mainly contains titanomagnetite, with a small amount of ilmenite and chlorite. Titanomagnetite is doped with vanadium, whose valency is mainly +3.

The decolorization of Acid Orange II mainly depended on degradation. Decreasing pH in acid range and increasing catalyst and hydrogen peroxide could accelerate the degradation. The presence of titanium and vanadium in magnetite greatly improved the catalytic activity of natural magnetite for the Acid Orange II decolorization. The whole decolorization process followed pseudo-first-order rate law, dominated by the heterogeneous Fenton reaction. The apparent pseudo-first-order rate constant k_{app} increased with the increase of the titanomagnetite content. During the degradation process, the naphthyl and benzene aromatic rings of Acid Orange II were gradually broken. The mineralization rate was about 30% 4 h after the degradation started. The natural vanadium–titanium magnetite has a good activity and stability.

Acknowledgements

This is contribution No. IS-1192 from GIG CAS.We would like to thank Beijing Synchrotron Radiation Facility for giving us the beam time for the XAFS measurement. This work is supported by National Natural Science Foundation of China (Grant No. 40773060) and "863" Exploration Program, the Ministry of Science and Technology of the People's Republic of China (Grant No. 2006AA03Z337).

References

[1] T.R. Giraldi, C.C. Arruda, G.M. da Costa, E. Longo, C. Ribeiro, Heterogeneous Fenton reactants: a study of the behavior of iron oxide nanoparticles obtained by the polymeric precursor method, J. Sol–Gel Sci. Technol. 52 (2009) 299–303.
[2] Y. Flores, R. Flores, A.A. Gallegos, Heterogeneous catalysis in the Fenton-type system reactive black 5/H_2O_2, J. Mol. Catal. A: Chem. 281 (2008) 184–191.
[3] R. Andreozzi, M. Canterino, V. Caprio, A. Di Sornma, R. Marotta, Use of an amorphous iron oxide hydrated as catalyst for hydrogen peroxide oxidation of ferulic acid in water, J. Hazard. Mater. 152 (2008) 870–875.
[4] S. Lee, J. Oh, Y. Park, Degradation of phenol with fenton-like treatment by using heterogeneous catalyst (modified iron oxide) and hydrogen peroxide, Bull. Korean Chem. Soc. 27 (2006) 489–494.
[5] V. Guzsvány, N. Banić, Z. Papp, F. Gaál, B. Abramović, Comparison of different iron-based catalysts for photocatalytic removal of imidacloprid, reaction kinetics, Mech. Catal. 99 (2010) 225–233.
[6] J.J. Wu, M. Muruganandham, J.S. Yang, S.S. Lin, Oxidation of DMSO on goethite catalyst in the presence of H_2O_2 at neutral pH, Catal. Commun. 7 (2006) 901–906.
[7] A. Romero, A. Santos, F. Vicente, Chemical oxidation of 2,4-dimethylphenol in soil by heterogeneous Fenton process, J. Hazard. Mater. 162 (2009) 785–790.
[8] L.C.A. Oliveira, M. Goncalves, M.C. Guerreiro, T.C. Ramalho, J.D. Fabris, M.C. Pereira, K. Sapag, A new catalyst material based on niobia/iron oxide composite on the oxidation of organic contaminants in water via heterogeneous Fenton mechanisms, Appl. Catal. A: Gen. 316 (2007) 117–124.
[9] R. Matta, K. Hanna, S. Chiron, Fenton-like oxidation of 2,4,6-trinitrotoluene using different iron minerals, Sci. Total Environ. 385 (2007) 242–251.
[10] H.H. Huang, M.C. Lu, J.N. Chen, Catalytic decomposition of hydrogen peroxide and 2-chlorophenol with iron oxides, Water Res. 35 (2001) 2291–2299.
[11] P. Baldrian, V. Merhautova, J. Gabriel, F. Nerud, P. Stopka, M. Hruby, M.J. Benes, Decolorization of synthetic dyes by hydrogen peroxide with heterogeneous catalysis by mixed iron oxides, Appl. Catal. B: Environ. 66 (2006) 258–264.
[12] E.G. Garrido-Ramirez, B.K.G. Theng, M.L. Mora, Clays and oxide minerals as catalysts and nanocatalysts in Fenton-like reactions – a review, Appl. Clay Sci. 47 (2010) 182–192.
[13] A.P.F.M. de Urzedo, C.C. Nascentes, R. Augusti, Degradation of the insecticides thiamethoxam and imidacloprid in aqueous solution as promoted by an innovative Fe-o/Fe_3O_4 composite, J. Braz. Chem. Soc. 20 (2009) 51–56.
[14] R.C.C. Costa, M.F.F. Lelis, L.C.A. Oliveira, J.D. Fabris, J.D. Ardisson, R.R.V.A. Rios, C.N. Silva, R.M. Lago, Novel active heterogeneous Fenton system based on $Fe_{3-x}M_xO_4$ (Fe, Co, Mn, Ni): the role of M^{2+} species on the reactivity towards H_2O_2 reactions, J. Hazard. Mater. 129 (2006) 171–178.
[15] R.C. Wu, J.H. Qu, Removal of azo dye from water by magnetite adsorption–fenton oxidation, Water Environ. Res. 76 (2004) 2637–2642.
[16] X.F. Xue, K. Hanna, C. Despas, F. Wu, N.S. Deng, Effect of chelating agent on the oxidation rate of PCP in the magnetite/H_2O_2 system at neutral pH, J. Mol. Catal. A: Chem. 311 (2009) 29–35.
[17] M. Hermanek, R. Zboril, N. Medrik, J. Pechousek, C. Gregor, Catalytic efficiency of iron(III) oxides in decomposition of hydrogen peroxide: competition between the surface area and crystallinity of nanoparticles, J. Am. Chem. Soc. 129 (2007) 10929–10936.
[18] M. Sorescu, L. Diamandescu, R.A. Brand, D. Tarabasanu-Mihaila, Mossbauer study of manganese-doped magnetite below the Verwey transition, Mater. Lett. 58 (2004) 885–888.
[19] F. Magalhaes, M.C. Pereira, S.E.C. Botrel, J.D. Fabris, W.A. Macedo, R. Mendonca, R.M. Lago, L.C.A. Oliveira, Cr-containing magnetites $Fe_{3-x}Cr_xO_4$: the role of Cr^{3+} and Fe^{2+} on the stability and reactivity towards H_2O_2 reactions, Appl. Catal. A: Gen. 332 (2007) 115–123.
[20] V.S. Coker, C.I. Pearce, R.A.D. Pattrick, G. Van der Laan, N.D. Telling, J.M. Charnock, E. Arenholz, J.R. Lloyd, Probing the site occupancies of Co-, Ni-, and Mn-substituted biogenic magnetite using XAS and XMCD, Am. Mineral. 93 (2008) 1119–1132.
[21] K.N. Pang, M.F. Zhou, Y.X. Ma, Fe–Ti–V oxide mineralization in the Permian Panzhihua gabbro, Emeishan Large Igneous Province, SW China, in: Mineral Deposit Research: Meeting the Global Challenge, vols. 1 and 2, 2005, pp. 453–456.
[22] C.G. Ramankutty, S. Sugunan, Surface properties and catalytic activity of ferrospinels of nickel, cobalt and copper, prepared by soft chemical methods, Appl. Catal. A: Gen. 218 (2001) 39–51.
[23] L. Menini, M.J. da Silva, M.F.F. Lelis, J.D. Fabris, R.M. Lago, E.V. Gusevskaya, Novel solvent free liquid-phase oxidation of beta-pinene over heterogeneous catalysts based on $Fe_{3-x}M_xO_4$ (M = Co and Mn), Appl. Catal. A: Gen. 269 (2004) 117–121.
[24] B.R. Petigara, N.V. Blough, A.C. Mignerey, Mechanisms of hydrogen peroxide decomposition in soils, Environ. Sci. Technol. 36 (2002) 639–645.
[25] W. Yu, T.L. Zhang, J.G. Zhang, X.J. Qiao, L. Yang, Y.H. Liu, The synthesis of octahedral nanoparticles of magnetite, Mater. Lett. 60 (2006) 2998–3001.
[26] S.J. Yang, H.P. He, D.Q. Wu, D. Chen, Y.H. Ma, X.L. Li, J.X. Zhu, P. Yuan, Degradation of methylene blue by heterogeneous Fenton reaction using titanomagnetite at neutral pH values: process and affecting factors, Ind. Eng. Chem. Res. 48 (2009) 9915–9921.
[27] J.X. Chen, L.Z. Zhu, UV-Fenton discolouration and mineralization of Orange II over hydroxyl-Fe-pillared bentonite, J. Photochem. Photobiol. A 188 (2007) 56–64.
[28] J.Y. Feng, X.J. Hu, P.L. Yue, Discoloration and mineralization of orange II using different heterogeneous catalysts containing Fe: a comparative study, Environ. Sci. Technol. 38 (2004) 5773–5778.
[29] R. Andreozzi, A. D'Apuzzo, R. Marotta, Oxidation of aromatic substrates in water/goethite slurry by means of hydrogen peroxide, Water Res. 36 (2002) 4691–4698.
[30] I.L. Junior, J.M.M. Millet, M. Aouine, M. do Carmo Rangel, The role of vanadium on the properties of iron based catalysts for the water gas shift reaction, Appl. Catal. A: Gen. 283 (2005) 91–98.
[31] K.J. Kim, S.L. Choi, J.H. Lee, H.J. Lee, J.Y. Park, Variations of the electronic, optical and magnetic properties caused by V doping in magnetite thin films, J. Korean Phys. Soc. 51 (2007) 1138–1142.
[32] M.F. Zhou, C.Y. Wang, K.N. Pang, G.J. Shellnutt, Y. Ma, Origin of giant Fe–Ti–V oxide deposits in layered gabbroic intrusions, Pan-Xi district, Sichuan province, SW China, in: Mineral Deposit Research: Meeting the Global Challenge, vols. 1 and 2, 2005, pp. 511–513.
[33] P. Chaurand, J. Rose, V. Briois, M. Salome, O. Proux, V. Nassif, L. Olivi, J. Susini, J.L. Hazemann, J.Y. Bottero, New methodological approach for the vanadium K-edge X-ray absorption near-edge structure interpretation: application to the speciation of vanadium in oxide phases from steel slag, J. Phys. Chem. B 111 (2007) 5101–5110.
[34] N. Guigue-Millot, Y. Champion, M.J. Hytch, F. Bernard, S. Begin-Colin, P. Perriat, Chemical heterogeneities in nanometric titanomagnetites prepared by soft chemistry and studied ex situ: evidence for Fe-segregation and oxidation kinetics, J. Phys. Chem. B 105 (2001) 7125–7132.
[35] M. Mohapatra, B. Pandey, C. Upadhyay, S. Anand, R.P. Das, H.C. Verma, Effect of Ni doping on the properties of fine magnetite particles, J. Magn. Magn. Mater. 295 (2005) 44–50.
[36] N.S. Gajbhiye, G. Balaji, S. Bhattacharyya, M. Ghafari, Mossbauer studies of nanosize $CuFe_2O_4$ particles, Hyperfine Interact. 156 (2004) 57–61.
[37] F.C.C. Moura, G.C. Oliveira, M.H. Araujo, J.D. Ardisson, W.A.A. Macedo, R.M. Lago, Highly reactive species formed by interface reaction between Fe-0-iron oxides particles: an efficient electron transfer system for environmental applications, Appl. Catal. A: Gen. 307 (2006) 195–204.
[38] R.J. Watts, M.K. Foget, S.H. Kong, A.L. Teel, Hydrogen peroxide decomposition in model subsurface systems, J. Hazard. Mater. 69 (1999) 229–243.
[39] G.T. Li, J.H. Qu, X.W. Zhang, H.J. Liu, H.N. Liu, Electrochemically assisted photocatalytic degradation of Orange II: influence of initial pH values, J. Mol. Catal. A: Chem. 259 (2006) 238–244.
[40] R. Andreozzi, V. Caprio, R. Marotta, Oxidation of 3,4-dihydroxybenzoic acid by means of hydrogen peroxide in aqueous goethite slurry, Water Res. 36 (2002) 2761–2768.
[41] L. Abramian, H. El-Rassy, Adsorption kinetics and thermodynamics of azo-dye Orange II onto highly porous titania aerogel, Chem. Eng. J. 150 (2009) 403–410.

[42] J.H. Ramirez, F.J. Maldonado-Hodar, A.F. Perez-Cadenas, C. Moreno-Castilla, C.A. Costa, L.M. Madeira, Azo-dye Orange II degradation by heterogeneous Fenton-like reaction using carbon–Fe catalysts, Appl. Catal. B: Environ. 75 (2007) 312–323.
[43] S.S. Chou, C.P. Huang, Application of a supported iron oxyhydroxide catalyst in oxidation of benzoic acid by hydrogen peroxide, Chemosphere 38 (1999) 2719–2731.
[44] J. Feng, X.J. Hu, P.L. Yue, Novel bentonite clay-based Fe-nanocomposite as a heterogeneous catalyst for photo-fenton discoloration and mineralization of orange II, Environ. Sci. Technol. 38 (2004) 269–275.
[45] W.P. Kwan, B.M. Voelker, Rates of hydroxyl radical generation and organic compound oxidation in mineral-catalyzed Fenton-like systems, Environ. Sci. Technol. 37 (2003) 1150–1158.
[46] R.V. Lloyd, P.M. Hanna, R.P. Mason, The origin of the hydroxyl radical oxygen in the Fenton reaction, Free Radic. Biol. Med. 22 (1997) 885–888.
[47] J. De Laat, H. Gallard, Catalytic decomposition of hydrogen peroxide by Fe(III) in homogeneous aqueous solution: mechanism and kinetic modeling, Environ. Sci. Technol. 33 (1999) 2726–2732.
[48] R. Matta, K. Hanna, T. Kone, S. Chiron, Oxidation of 2,4,6-trinitrotoluene in the presence of different iron-bearing minerals at neutral pH, Chem. Eng. J. 144 (2008) 453–458.
[49] R.C.C. Costa, M. de Fatima, F. Lelis, L.C.A. Oliveira, J.D. Fabris, J.D. Ardisson, R.R.V.A. Rios, C.N. Silva, R.M. Lago, Remarkable effect of Co and Mn on the activity of $Fe_{3-x}M_xO_4$ promoted oxidation of organic contaminants in aqueous medium with H_2O_2, Catal. Commun. 4 (2003) 525–529.
[50] S.S. Lin, M.D. Gurol, Catalytic decomposition of hydrogen peroxide on iron oxide: kinetics, mechanism, and implications, Environ. Sci. Technol. 32 (1998) 1417–1423.
[51] S.S. Chou, C.P. Huang, Y.H. Huang, Heterogeneous and homogeneous catalytic oxidation by supported gamma-FeOOH in a fluidized bed reactor: kinetic approach, Environ. Sci. Technol. 35 (2001) 1247–1251.
[52] J.Y. Feng, X.J. Hu, P.L. Yue, H.Y. Zhu, G.Q. Lu, Discoloration and mineralization of Reactive Red HE-3B by heterogeneous photo-Fenton reaction, Water Res. 37 (2003) 3776–3784.
[53] Y. Mu, H.Q. Yu, J.C. Zheng, S.J. Zhang, TiO_2-mediated photocatalytic degradation of Orange II with the presence of Mn^{2+} in solution, J. Photochem. Photobiol. A 163 (2004) 311–316.
[54] J.H. Deng, J.Y. Jiang, Y.Y. Zhang, X.P. Lin, C.M. Du, Y. Xiong, $FeVO_4$ as a highly active heterogeneous Fenton-like catalyst towards the degradation of Orange II, Appl. Catal. B: Environ. 84 (2008) 468–473.